4. Finite Element Modelling Strategies

4.1. Introduction

In this chapter, a 3D wheel/IRJ FE contact-impact model is reported. Some simplification strategies are employed to reduce the model size. The exact geometry, material zones, boundary conditions and loading are simplified in the idealised model presented. The wheel-IRJ railhead contact is first established in the static analysis and the results transferred to dynamic analysis for impact simulations. Details of contact modelling in both the static and the dynamic procedures are also presented. Numerical examples of the static/dynamic FE model is reported in Chapter 5.

4.2. Complexities of Modelling IRJ

It is fairly complex to simulate the behaviour of an IRJ that works under the dynamic environment of wheel passages. The dynamics of the IRJ are affected by the characteristics of the rolling stock and that of the IRJ itself. The dynamics of the rolling stock is idealised as pure rolling/sliding of the wheel; only a single wheel with a proportional wagon mass is modelled. The complexities of modelling the IRJ can be illustrated through the discussion of geometry, material and boundary condition.

4.2.1. Geometry

The conventional IRJ used in Australia consists of rails, joint bars, bolts, washers and nuts and insulation materials for joint bars and end post (Fig. 4.1).

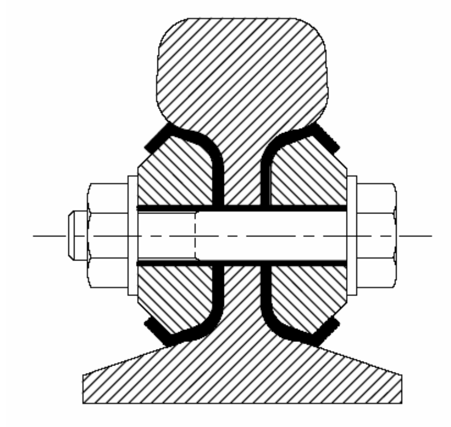

(a) Cross section of IRJ

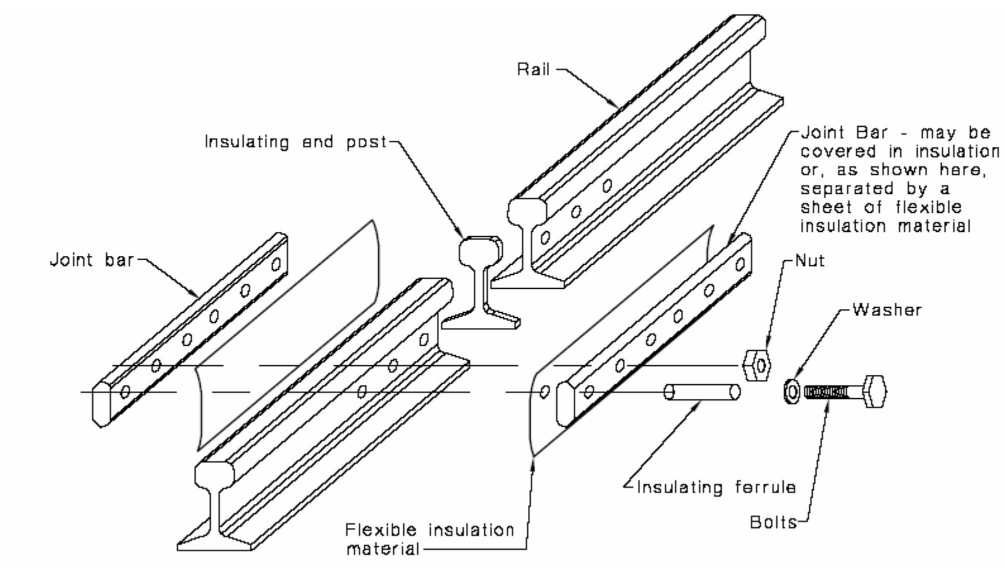

(b) Exploded view

Figure 4.1 Typical insulated rail joint assembly (AS1085.12, 2002)

This thesis considers the IRJ that consists of AS 60kg rail (Fig. 4.2) and joint bar (Fig 4.3) connected by M24 bolt (Fig. 4.4).

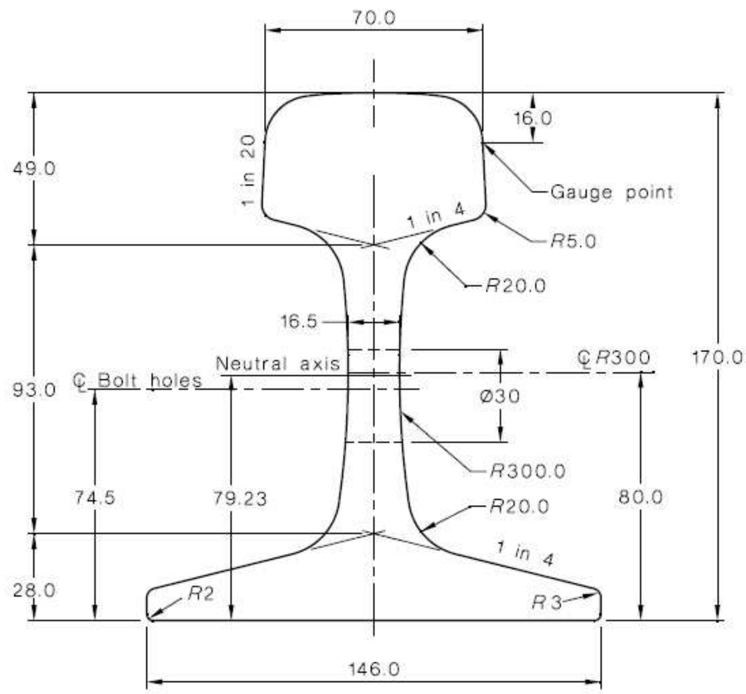

Figure 4.2 60kg Rail dimension (Standards Australia, 2002)

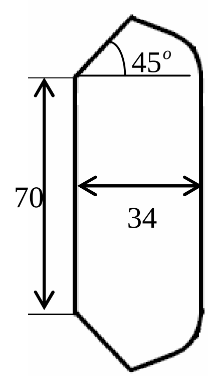

Figure 4.3 Joint bar dimensions

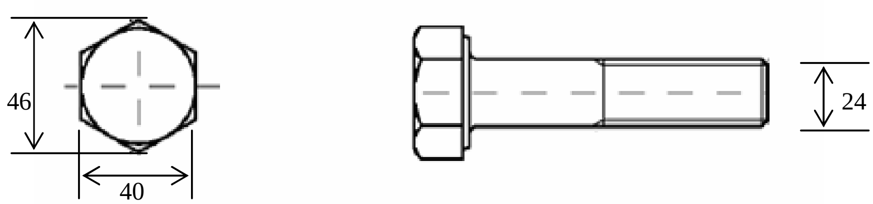

Figure 4.4 M24 Bolt dimensions (Standard Australia & Standard New Zealand, 1996)

As illustrated in Fig. 4.5, the wheel tread and hub is designed to withstand heavy loading due to contact forces and axle loading. The thin wheel web reduces the wheel mass and the wheel flange is necessary to provide guidance along curved track.

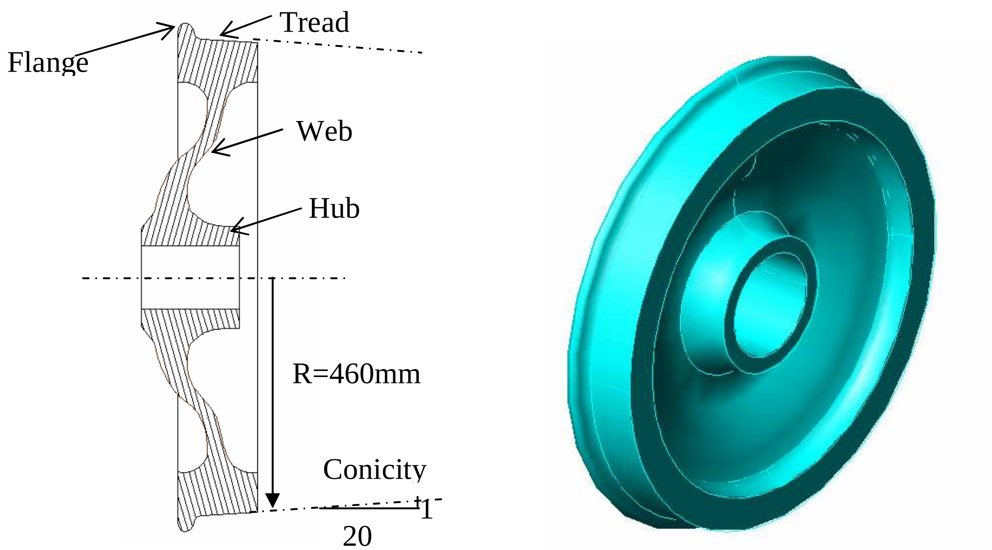

Figure 4.5 Geometry of wheel

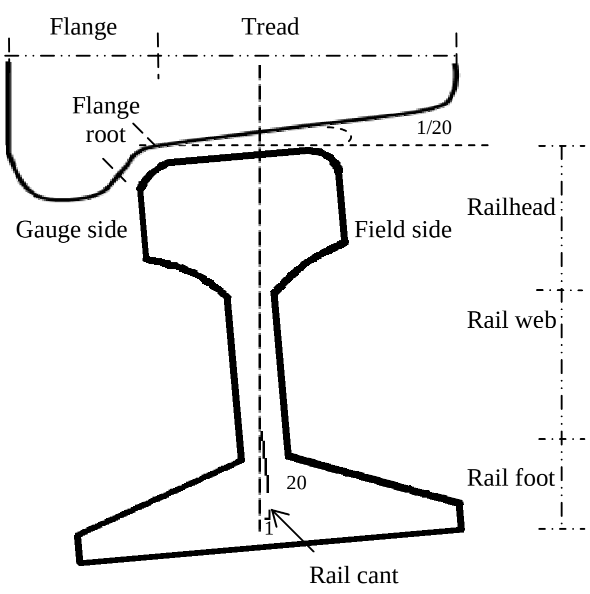

Figure 4.6 Rail/wheel vertical section alignment

The wheel profile without any wear or flat is perfectly conical with the conicity of 1/20. The vertical axis of IRJs also has an inclination of 1/20. Fig. 4.6 illustrates the alignment of the rail to maintain its contact to the wheel.

4.2.2. Material

The wheel and the rail material (steel) is assigned elasto-plastic properties. Table 4.1 lists the mechanical properties of steel and insulation material Nylon66:

Table 4.1 Mechanical property of steel and insulation material (Chen, 2002)

Property	*Steel*	*Nylon66*
Young's modulus	210GPa	1.59GPa
Poisson's ratio	0.3	0.39
Density	7800kg/ m^3	1140kg/ m^3
Yield Stress	780MPa	(elastic only)

4.2.3. Boundary Conditions

Under pure rolling, the wheel rotates at an angular velocity ω that corresponds to the linear velocity v. The wheel motion is restrained in the lateral direction; in other words, DOFs 5 and 6 (Fig. 4.7) are arrested.

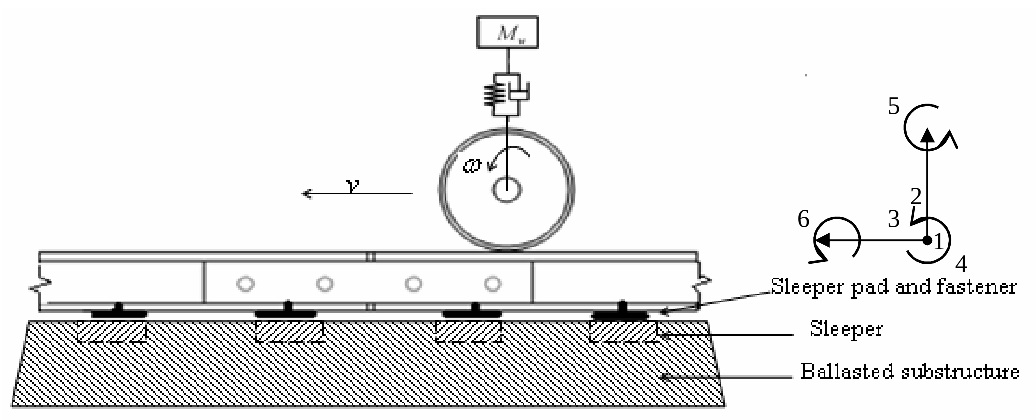

Figure 4.7 Boundary conditions of wheel and IRJ

The rail is positioned on the ballast bed using sleepers (prestressed concrete sleepers in this case) which are embedded into the ballast layer. Sleeper pads are inserted between the sleepers and the rail bottom and are fixed by the fastening system (see Fig. 4.8).

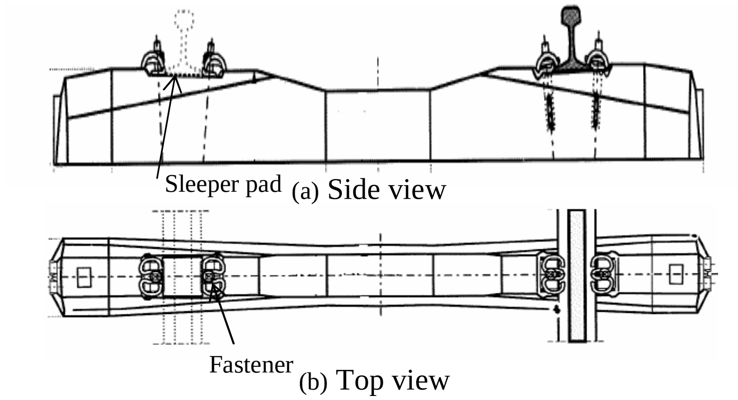

Figure 4.8 Typical prestressed concrete sleeper arrangement (Esveld, 2001)

In the longitudinal direction, the wheel load influences the rail deflection for a certain length. According to Sun (2003), referring to Fig. 4.9, the length is approximately 10m for AS 60kg rail subjected to a concentrated wheel load of 100KN. In this thesis, the length of rail being modelled is 12m which is sufficient for the load influence.

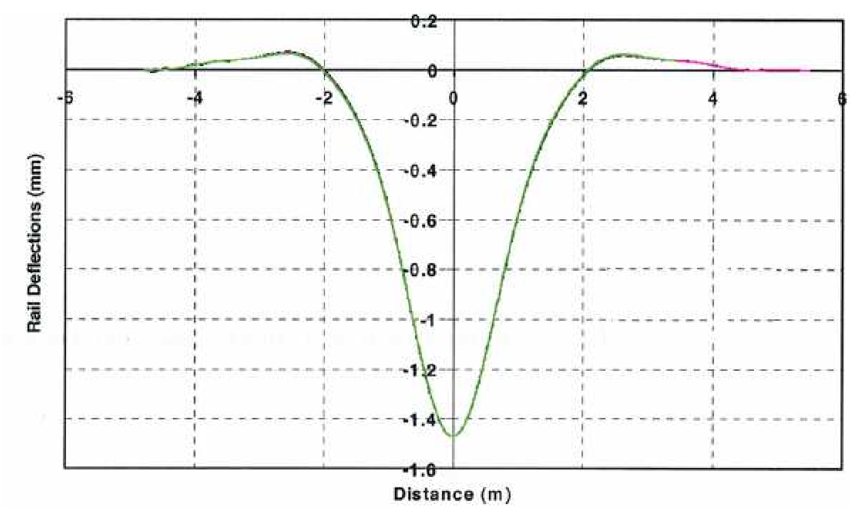

Figure 4.9 Rail effect length with deflection (Sun, 2003)

The wheel/rail contact is another boundary condition that provides restraint in both the vertical and horizontal directions.

4.3. Strategy-1: Simplifications of Geometry Modelling

The complexity of the IRJ and the wheel geometry demands simplifications to reduce the computational cost. For the IRJ, as attention is focused on the dynamics and failure of the railhead wheel contact impact area in the vicinity of the end post, the finite element model was simplified to just one part model by ignoring the interaction between the contact surfaces of the rail, the joint bars, the bolts, and the nuts. Furthermore, the bolt-heads and nuts are not essential and hence they are ignored. However, the bolt shank is retained to apply the pre-tension load. In other words, as shown in Fig.4.10, the fully assembled IRJ was assumed as one instance partitioned with varying material regions (insulation & rail steel materials). Although the simplified model can not predict failure modes such as bolt looseness and delamination, it has been found quite sufficient for the determination of contact impact forces of the railhead in the vicinity of the end post.

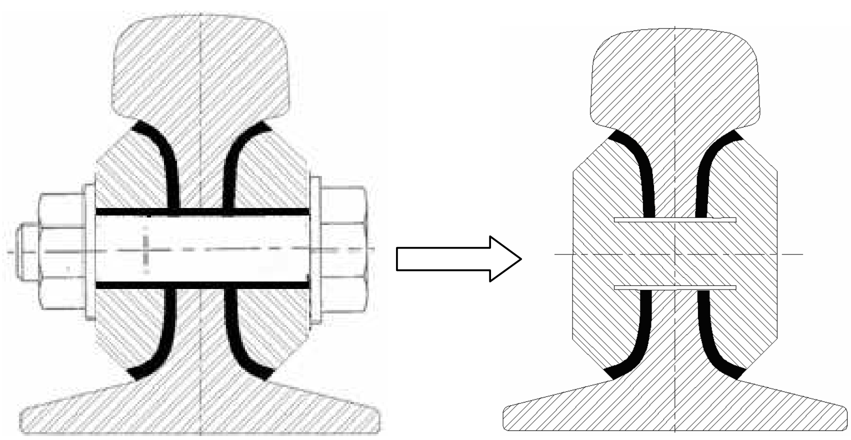

Figure 4.10 Idealisation of the IRJ geometry

Since this research focus is on the impact at IRJs and the function of the wheel is to provide a contact patch across the IRJ, the geometry of wheel cross-section is also simplified. Since the flange contact is out of our scope, the wheel flange is firstly removed and the wheel cross-section is also simplified as shown in Fig. 4.11. The wheel radius and tread conicity are kept the same as the design of 460mm and 1/20 respectively.

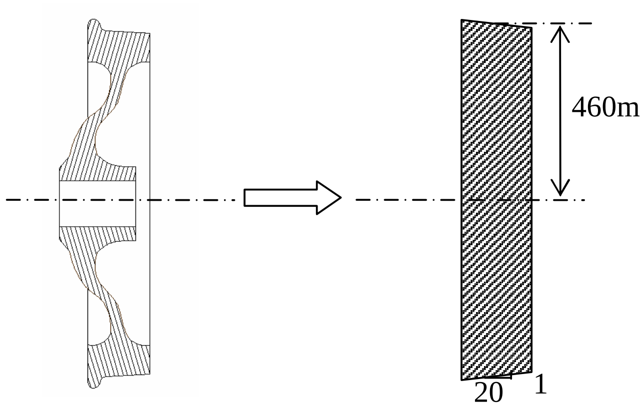

Figure 4.11 Wheel geometry simplification

As a result, the 3D full-scale FE model is generated as shown in Fig. 4.12based on the above idealised geometries of the IRJ and wheel.

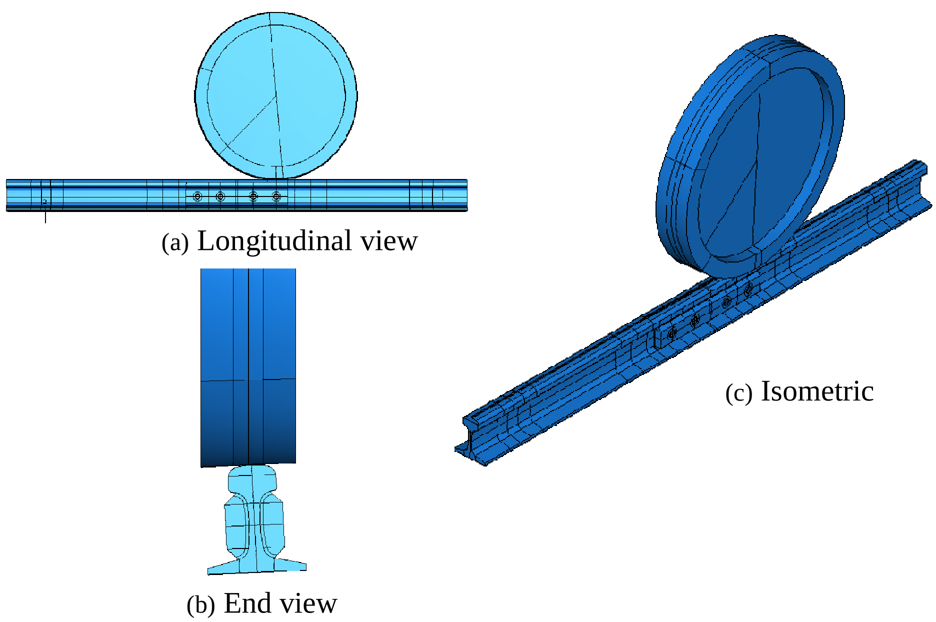

Figure 4.12 Geometry of FE model

4.4. Strategy-2: Simplifications of Material Modelling

Although steel is elasto-plastic, as the bulk of the rail section is subjected to very low levels of stresses under wheel passage, for all those regions steel is considered elastic. The zone close to the wheel contact patch is partitioned to assign elasto-plastic properties. The joint bar, bolt shank and bulk of the wheel steel are simply considered as elastic. A narrow strip of the wheel tread is assigned with elasto-plastic steel property. The end post and thin partition between the rail web and the joint bar are assigned Nylon66 properties that remained elastic.

4.4.1. Elasto-plastic steel zones

The elasto-plastic steel zone is limited to the vicinity of the end post close to the wheel/rail contact patch. The length of this zone is defined as the product of the longitudinal velocity of the wheel and the duration of the simulation. Correspondingly, the elasto-plastic zone of the wheel is a strip across the wheel tread as shown in Fig. 4.13.

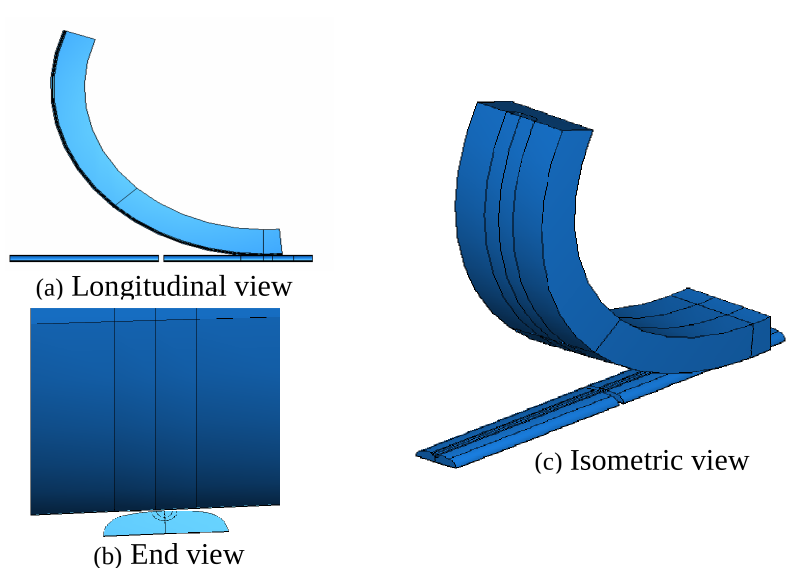

Figure 4.13 Elasto-plastic steel zone for wheel and IRJ

4.4.2. Insulating material zones

The insulating material zones are modelled for the rail end post insulation and joint bar/rail insulations. As the geometry has been simplified, the insulation between the bolt shank and rail web hole is ignored (rather a gap is provided between the surfaces of these two parts). Fig. 4.14 shows the insulating material zones of the IRJ.

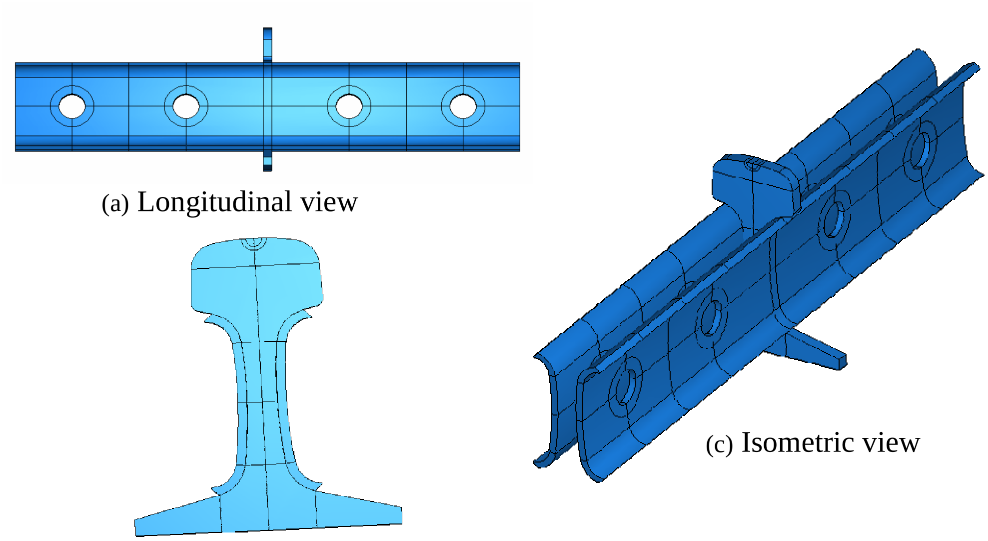

(a) Longitudinal view

(b) End view

(c) Isometric view

Figure 4.14 Insulation zone of IRJ

4.5. Strategy-3: Simplifications of Boundary Conditions

The IRJ is supported on the ballasted substructure through sleepers and sleeper pads at the rail bottom. Modelling such a mechanical system is very expensive and unnecessary, particularly for this research that is focused on the impact at the railhead. To reduce the computational cost, some simplifications are made for modelling the sleepers, the sleeper pads, the fasteners and the ballasted substructure. In the longitudinal direction, the rail end boundary condition is also simplified.

4.5.1. Idealisation of support system

The function of sleepers is to support the rail and transfer the loading to the substructure. The rail bottom is fixed to the sleeper by the fastener and the sleeper pad is used to minimise the damage to the sleeper top surface. For the IRJ, the interactive surfaces with the sleepers are restrained in all directions. Sleeper itself was simplified as a spring and dashpot.

The rail support system is modelled as shown in Fig. 4.15. The interaction of the rail bottom surface and the sleeper top surface is modelled through coupling at a single reference point that has six DOFs of which five DOFs except the vertical displacement DOF are arrested. The effective area that represents the coupling zone is determined as the product of the top width (136mm) of the prestressed concrete sleeper and the width of the rail base (146mm). The sleepers are spaced at 700mm. The stiffness and damping of the support system are combined with that of the substructure.

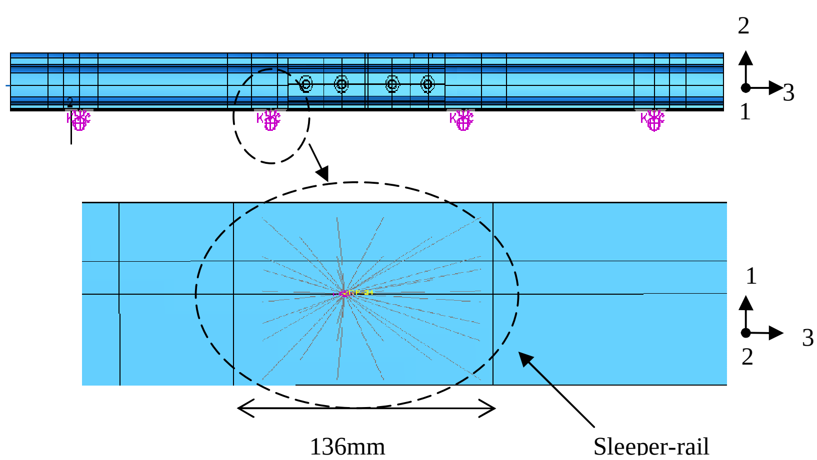

Figure 4.15 Sleeper support idealisation

4.5.2. Elastic support

The property of ballast substructure is non-linear and complicated. To set up a model of reasonable size, the ballast substructure is usually simplified as an elastic layer. There are several models reported in the literature that treat ballast as an elastic support (Zhai (1996), Newton and Clark (1979), Fermer and Nielsen(1995)). In this research, a linear single layer model is employed as shown in Fig. 4.16. One end of each spring/dashpot element is connected to the reference node (Fig. 4.16) and the other end is fixed to the ground.

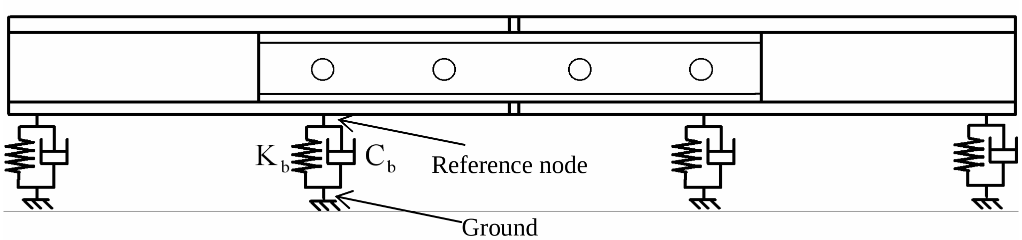

Figure 4.16 One-layer rail elastic support model

4.5.3. Beam element to solid element connections

As described in section 4.2, to truly account for the effect of wheel loading, a 12m long rail is necessary for the system considered. It is very expensive to model the 12m long rail using 3D solid elements. Hence, a beam element is employed to model a segment of 9.6m long rail and the remaining 2.4m rail in the vicinity of the end post is modelled using solid elements. Therefore, it becomes essential to ensure proper connection between the beam elements and the solid elements.

Each end of the rail section of solid element, is assumed to be a rigid surface disregarding shear deformation. The beam element is positioned in such a way that its geometric centre coincides with the geometric centre of the rail section modelled with solid elements.

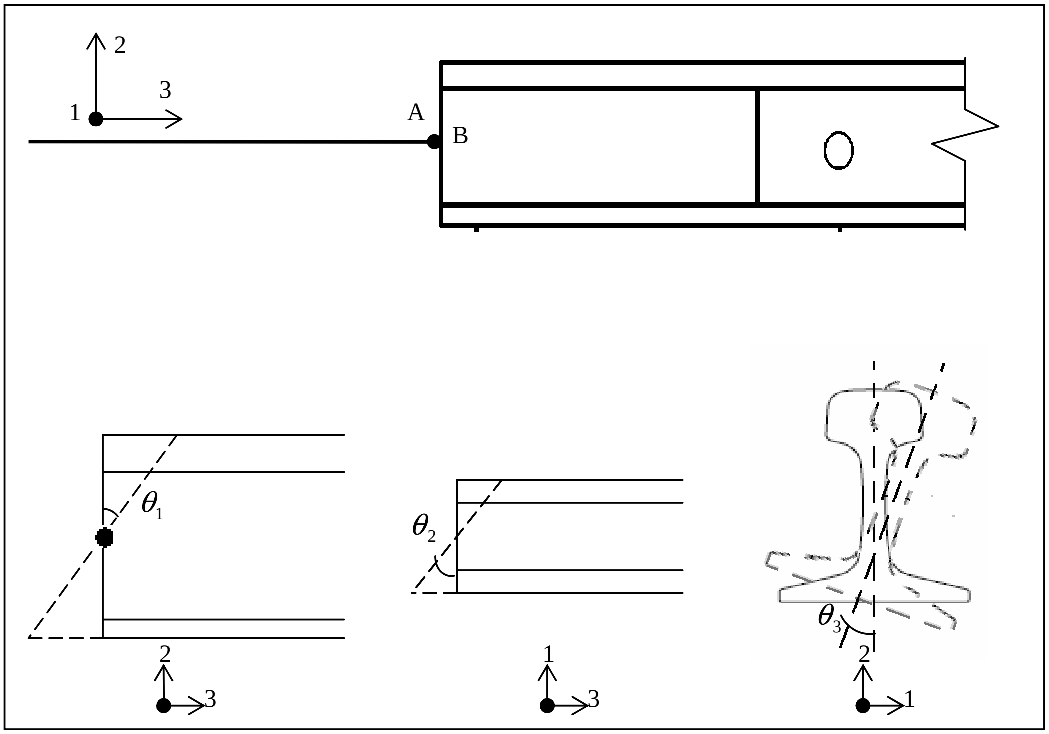

Figure 4.17. Beam-solid element connection

Referring to Fig. 4.17, the nodes A and B belong to the beam element and the solid element respectively. The six DOFs of the beam element node A $u_{1A}, u_{2A}, u_{3A}, u_{4A}, u_{5A}, u_{6A}$ are related to the three DOFs of the solid element nodes u_{1B}, u_{2B}, u_{3B} as shown in Eq. (4.1).

$$\begin{cases} u_{1A} = u_{1B} \\ u_{2A} = u_{2B} \\ u_{3A} = u_{3B} \\ u_{4A} = \theta_1 \\ u_{5A} = \theta_2 \\ u_{6A} = \theta_3 \end{cases} \tag{4.1}$$

where $\theta_1, \theta_2, \theta_3$ are rail section rotation about the geometric centre and defined by Eq.(4.2) as the quotient of several controlling node displacements and their distance to the geometric centre as shown in Fig. 4.18. Nodes B, C, D are all in the rail section plane. Node B is the geometric centre of the rail section and Node C is located at the railhead surface centre and Node D is located at the rail web surface with the same vertical distance to the bottom as Node B.

$$\begin{cases} \theta_1 = (u_{3C} - u_{3B}) / d_{BC} \\ \theta_2 = (u_{3D} - u_{3B}) / d_{BD} \\ \theta_3 = (u_{1C} - u_{1B}) / d_{BC} \end{cases} \tag{4.2}$$

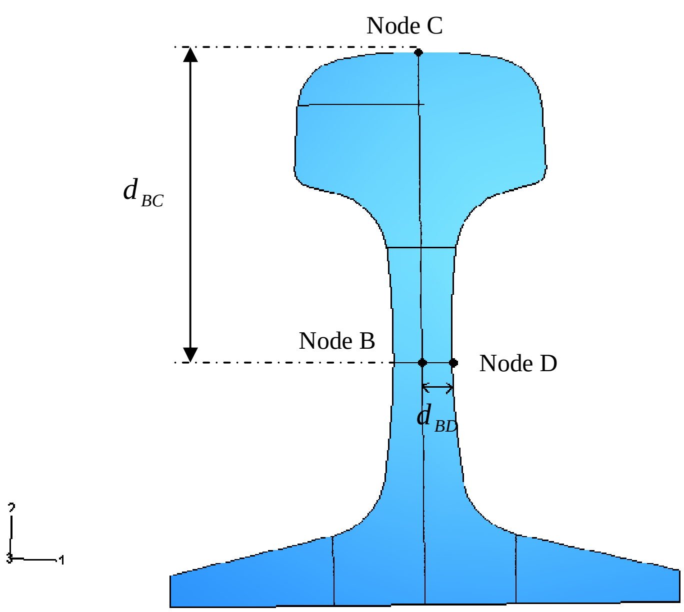

Figure 4.18 Controlling nodes for rail section rotational DOFs

Fig. 4.19 presents the beam-solid connection in the 3D model.

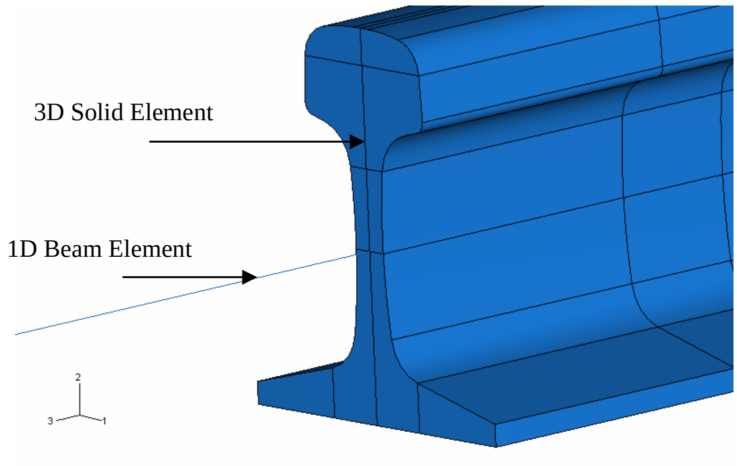

Figure 4.19 Beam-solid connection of 3D model

A schematic diagram of the full model of the IRJ is shown in Fig. 4.20.

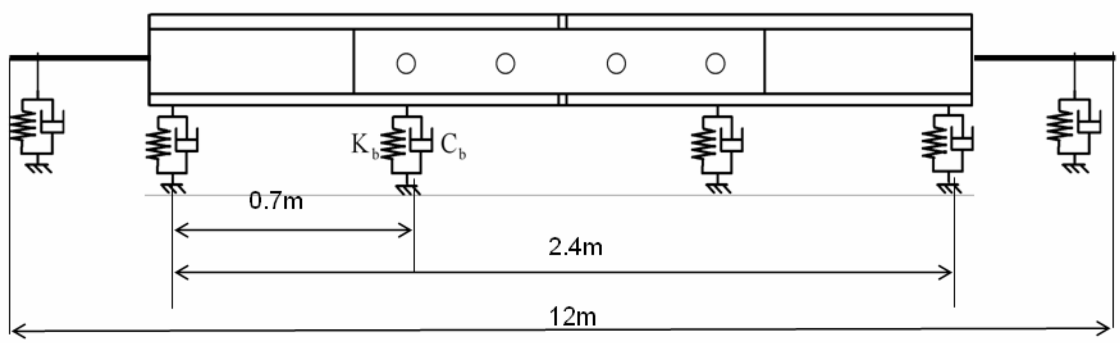

Figure 4.20 Schematic diagram of the full IRJ model

4.5.4. Boundary conditions of the wheel

Proportion of wagon mass is transferred to the wheel through the suspension system as shown in Fig. 4.21. The proportional mass is obtained by dividing the gross wagon mass by the number of wheels. Similar to the elastic support system, the suspension system is simplified into a single layer spring/damping model.

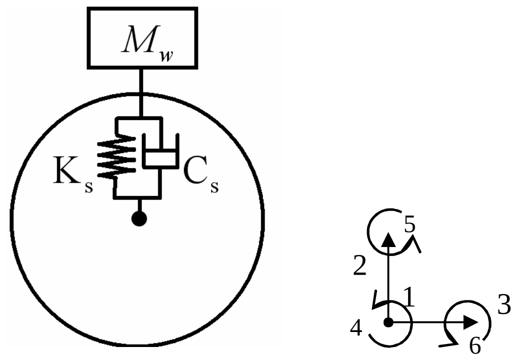

Figure 4.21 The wheel loading system

In the static wheel/rail contact model, the wheel DOF 2 is free and DOFs 1 and 3 are arrested. In the dynamic analysis, the lateral motion of the wheel is restrained to ensure the contact stability before impact. The wheel DOFs 2 and 3 are set free. For the pure rolling condition, the wheel body is assigned an initial condition of rotating speed ω around its centre axis and a longitudinal velocity v which is defined as the product of rotating speed and the radius.

For the pure sliding case (that models the brake force applied to the wheel causing wheel locking) the wheel is assigned with the longitudinal velocity v without the rotating speed ω. In other words, the wheel DOF 3 is set to the velocity of v, DOF 2 is free and DOFs 1, 4, 5, 6 are arrested.

4.6. Strategy-4: Loading Strategy

Prior to impact, the railhead and the wheel must attain a steady state of contact in order to ensure confidence in the solutions of the impact at the IRJ. Compared with the dynamic analysis using ABAQUS/Explicit, the static analysis employing ABAQUS/Standard has the advantage of attaining the steady state of contact with much cheaper computational cost. This strategy leads to a two-stage analysis for whee/rail contact impact at the IRJ.

In the static model, bolt pretension load, wheel axle load and the wheel centrifugal force are applied to the FE model. Bolt pretension load is applied through the internal cross section of the bolt shank, as shown in Fig. 4.22. Bolt pretension P_b is calculated from the bolt torque moment *T*, the bolt diameter *D* and the coefficient of the bolt torque moment K_b (K_b=0.19-0.25) as shown in Eq. (4.3).

$$P_b = \frac{T}{K_b D} \tag{4.3}$$

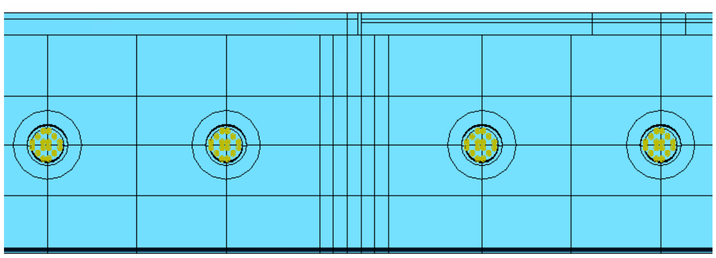

(a) Longitudinal view

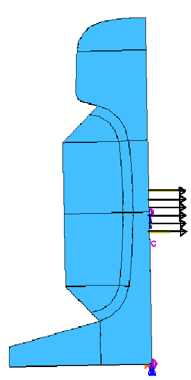

(b) End view

Figure 4.22 Bolt pretension load application

The wheel axle load is the weight of proportional wagon mass and applied to wheel centre, shown as Fig. 4.23. The wheel centrifugal force is employed to the static model as the preload of rotation. This was necessary as steady state rolling/sliding was desired in the dynamic analysis.

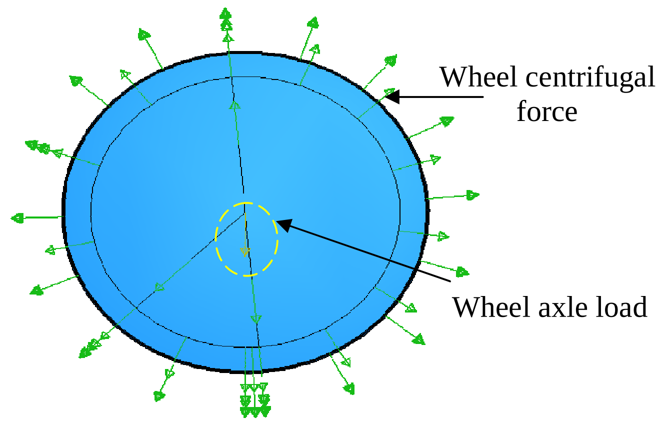

Figure 4.23 Wheel axle load and centrifugal force

4.7. Strategy-5: Wheel/Rail Contact Modelling

Definition of rail/wheel contact interaction in ABAQUS is very sensitive to convergence, accuracy of result, and computational time. Thus careful definition of the rail/wheel contact is the key to the impact dynamic analysis.

In the modelling, the master/slave contact surface method is employed for both the static and the dynamic analyses. The surfaces of the wheel are defined as the master, and the railhead is defined as the slave. The contact surface pair is allowed to undergo finite sliding. The interface friction is described with the Coulomb friction law by defining a friction coefficient μ . In the normal direction, the pressure-overclosure relationship is set to HARD meaning that surfaces transmit no contact pressure unless the nodes of the slave surface contact the master surface. Fig. 4.24 shows the contact surfaces of the wheel and the railhead.

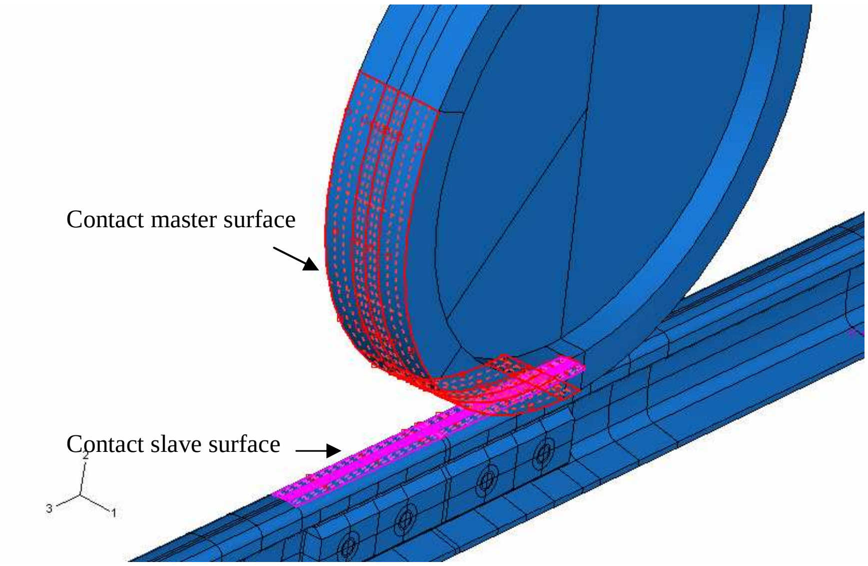

Figure 4.24 Contact surfaces for wheel and IRJ

4.7.1. Contact definition in static model

The Lagrange Multiplier method is used in static analysis for the contact constraint enforcement. Iterations continue until convergence of the solution is obtained. If a slave node penetrates the master surface by more than 0.1% of the characteristic interface length, which is the size of smallest element, the contact pressure is modified according to the penetration and another series of iterations is performed until convergence is once again achieved. Only when the penetration tolerance requirement is satisfied, is the solution accepted.

At the beginning of the contact analysis, there may exist small gaps or penetrations caused by numerical roundoff, or bad assemblies. Adjusting the initial position of the slave contact surface is required to eliminate these gaps or penetrations; otherwise, slave nodes that are overclosed in the initial configuration will remain overclosed at the start of the simulation, which may cause convergence problems. In static analysis, an adjustment zone is defined by specifying an adjusting depth a. The zone extending the distance a in the normal direction from the master surface is termed as the adjustment zone. Any nodes on the slave surface that are within the adjustment zone in the initial geometry of the model are moved precisely onto the master surface as shown in Fig.4.25. The motion of these slave nodes does not create any strain in the model; it is simply treated as a change in the geometry definition. When 'a' is too large, ill contact occurs leading to incorrect stress solutions, especially in the area around the contact surface. On the other hand, when 'a' is too small, contact iteration exhibits sensitivity to the mesh leading to convergence problems.

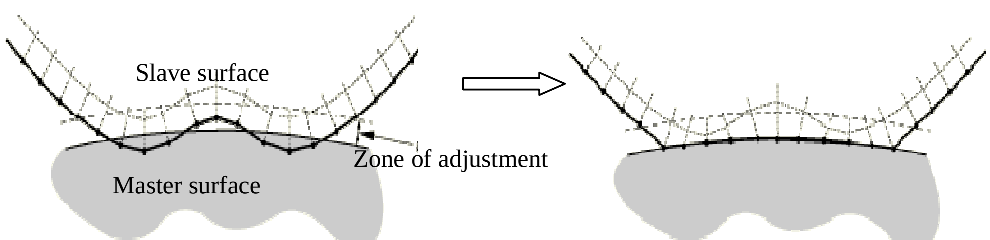

Figure 4.25 Contact surfaces initial adjustment (Abaqus, 2003)

To stabilise the numerical roundoff excited by the rigid body motion, the contact control parameter APPROACH is used to address the problem. This option activates viscous damping in the normal direction to prevent numerical difficulties associated with the rigid body motion that occurs when surfaces that are not initially in contact are brought into contact.

4.7.2. Contact definition in dynamic analysis

In ABAQUS/Explicit, two contact constraint enforcement methods, namely, the Penalty method and Kinematic method are available. Both methods were performed and results compared. The Penalty method is chosen because of the better performance (results are presented in the Chapter 5).

4.8. Strategy-6: Meshing

Meshing is an important part of FE modelling which has a strong influence on the reliability and accuracy of results as well as the model efficiency. Refined mesh usually provides more accurate results than coarse mesh. However the refined mesh increases the computational cost significantly. Hence, some meshing strategies are employed to set up a reliable FE model with reasonable cost. For the parts which undergo high level loading or stress, refined mesh is necessary. On the other hand, for the parts which are away from the severe loading or stress condition, coarse mesh is suitable to reduce the model size.

The whole FE model contains 3 major parts: wheel, IRJ solid part and IRJ beam part. For the wheel, the zone close to the wheel/rail contact patch is partitioned and assigned the refined mesh. The zone in the wheel tread is partitioned in such a way that a circle with 25mm radius extrudes along the wheel circumference as shown in Fig. 4.26 (a). Another partition is made in the wheel tread as shown in Fig. 4.27 (b). The circumference length of this partition is the product of wheel rotating velocity and simulation duration. The refined mesh is in the intersection zone of these two partitions with the element size of 2.5mm. The wheel meshing is presented as Fig. 4.27.

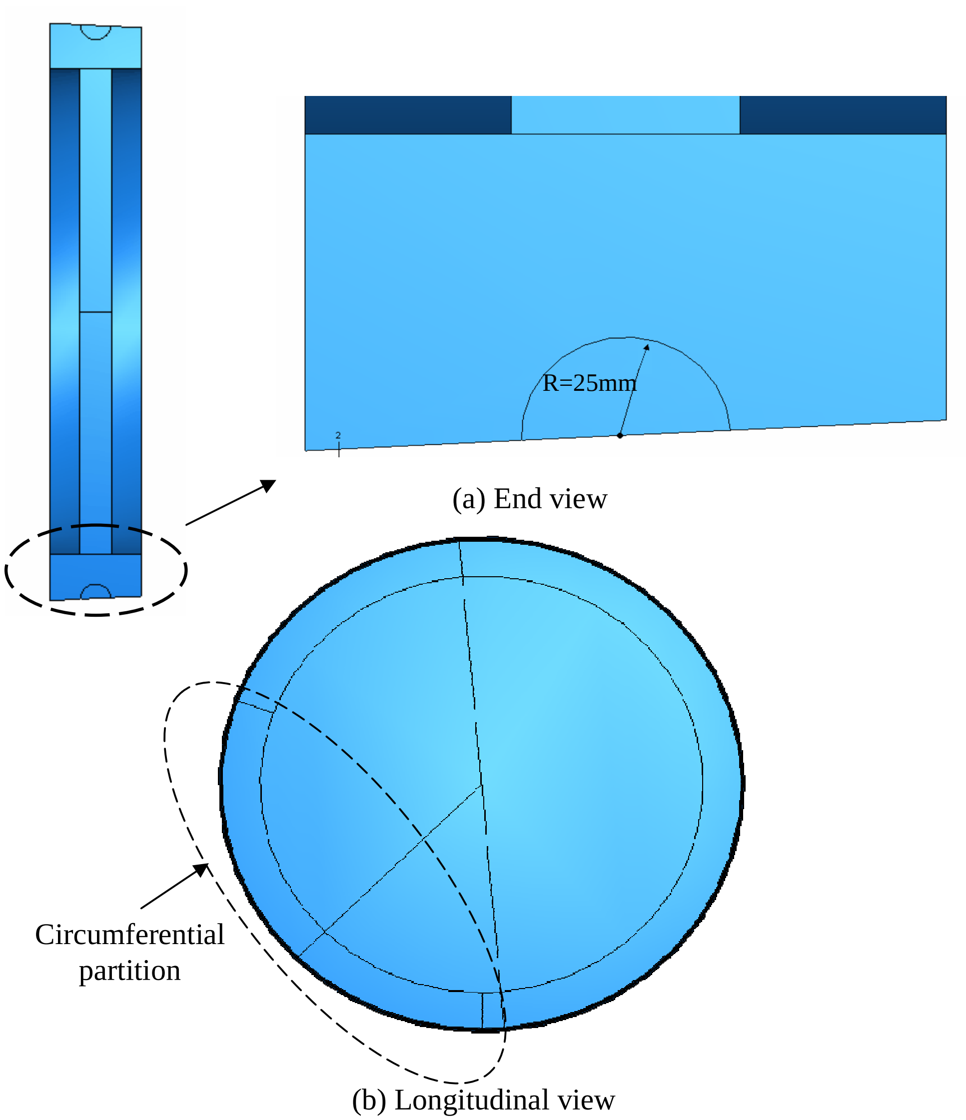

Figure 4.26 Wheel partition

The beam part for the IRJ is discretised using beam elements with a size of 200mm with a total number of 60. The two node linear Timoshenko shear flexible beam element B31 in the ABAQUS element library is employed with ABAQUS.

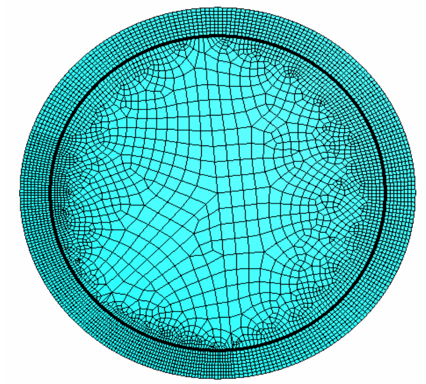

(a) Longitudinal view

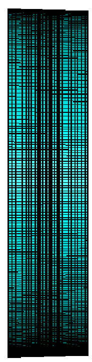

(b) End view

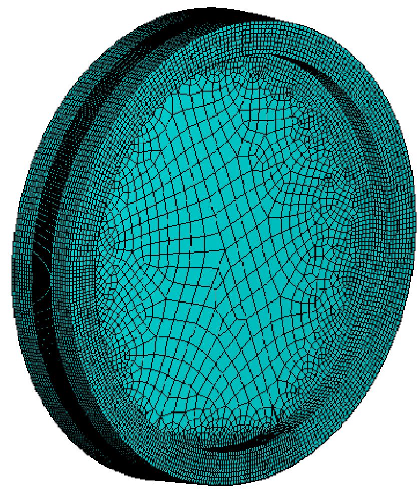

(c) Isometric view

Figure 4.27 Wheel meshing

The solid part of the IRJ consists of two major zones. One zone is part of the railhead in the vicinity of the end post with a longitudinal length of 658mm, referring to Fig. 4.28. The rail head zone is generally assigned with refined mesh with the element size of 4mm. A further partition is made in the central top part of the railhead to obtain a more refined mesh for the wheel/rail contact zone. In this zone the element size is approximately 0.5mm.

The rest of the IRJ (Fig. 4.30) is generally assigned with coarser mesh. The element size in this part, except the partition for bolt shank, is approximate 5mm. Because of the high level of bolt pretension load, the partition of bolt shank is assigned a refined mesh with the element size of 2.5mm. The partition for end post zone is also assigned with a refined mesh with an element size of 2.6mm.

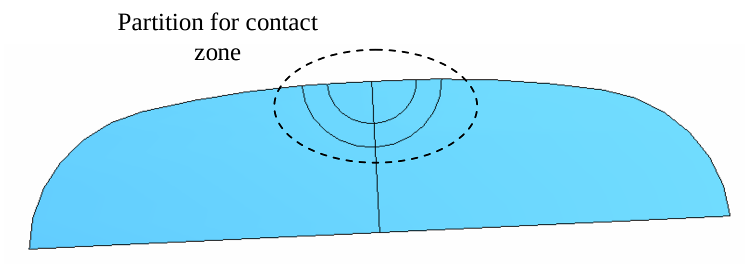

(a) End view

(b) Longitudinal view

Figure 4.28 Railhead zone of IRJ

The mesh of the railhead zone is shown in Fig. 4.29.

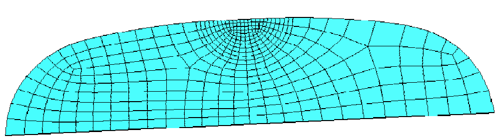

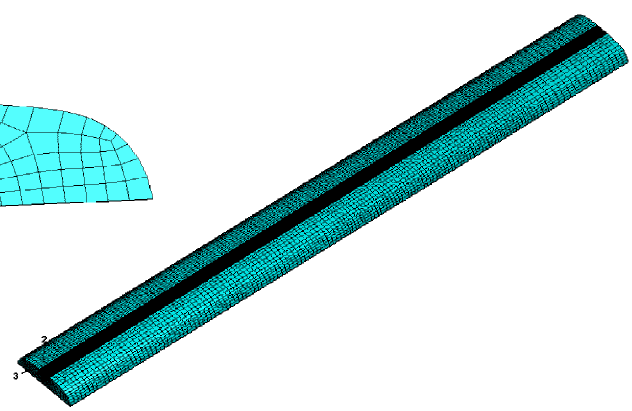

(a) End view

(b) Isometric view

Figure 4.29 Refined mesh for railhead zone of IRJ

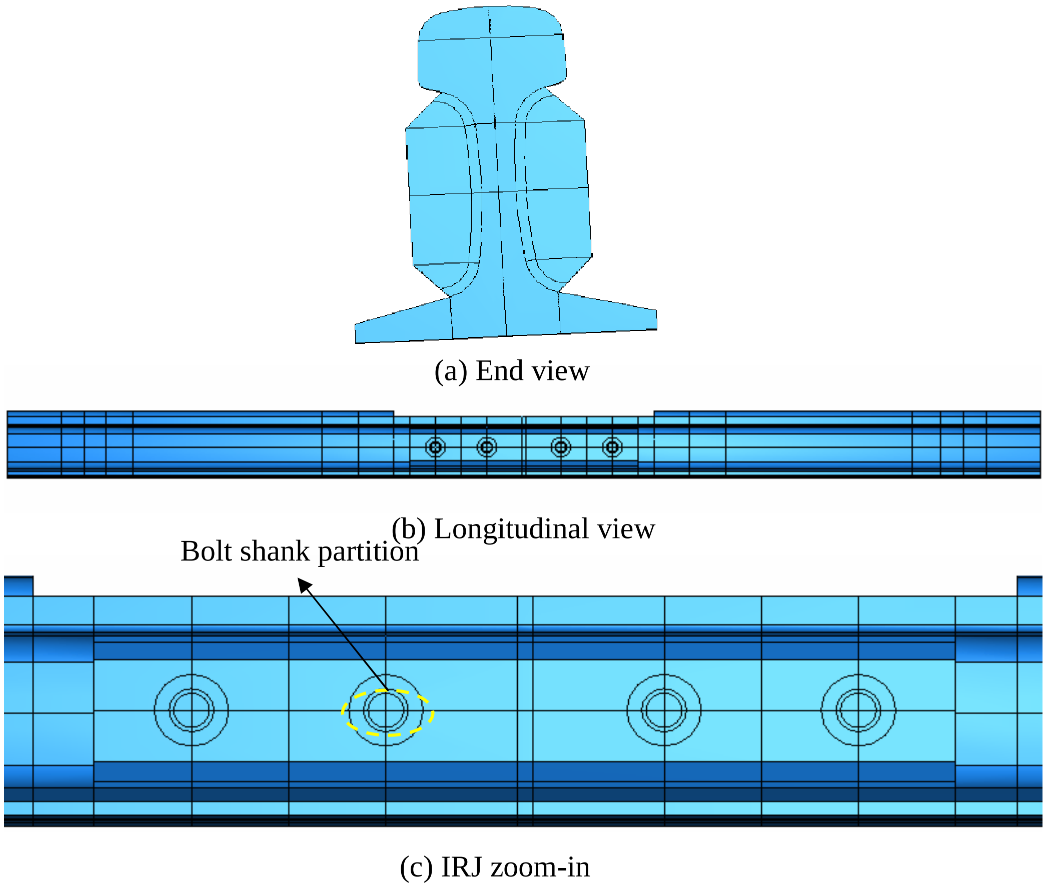

Figure 4.30 Remaining part of IRJ

The meshing of the IRJ without the railhead partition is presented in Fig 4.31. The railhead partition is connected to the other parts of the IRJ at their intersection surfaces using coupling technique. All 3 coupling DOFs on the surfaces are arrested.

The full FE wheel and IRJ contact model is presented as Fig. 4.32. The entire FE model consists of 169,655 nodes and 147,322 eight-node linear hexahedral solid elements with reduced integration C3D8R. Table 4.2 presents the mesh information for different parts.

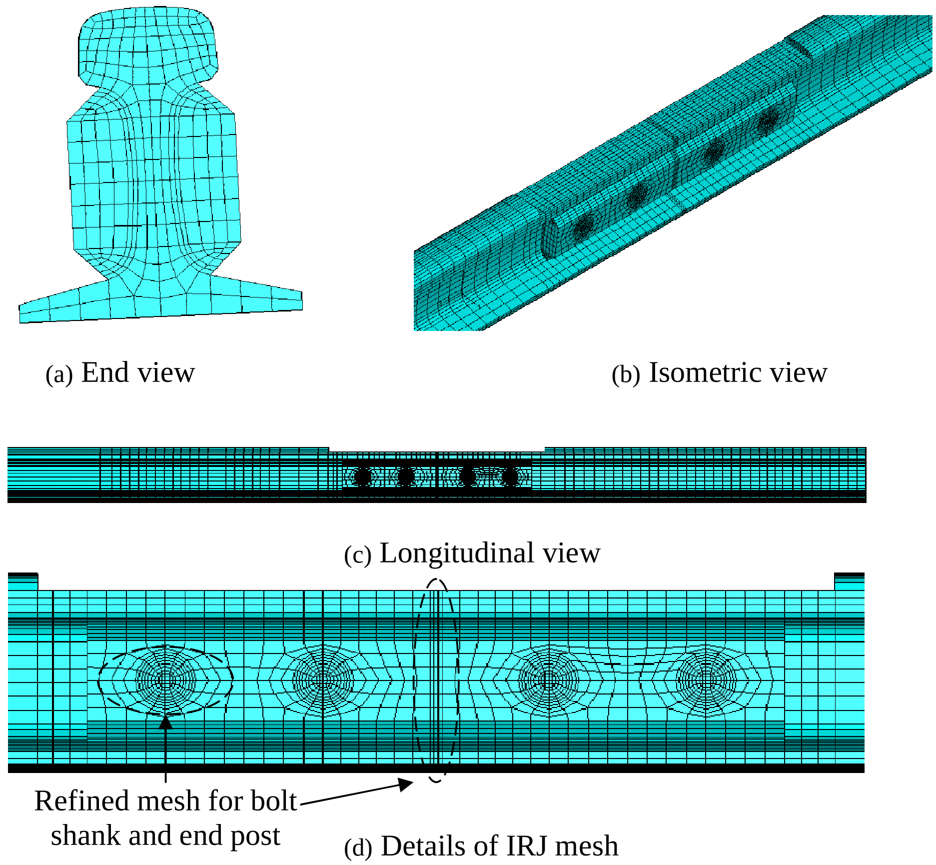

(a) End view (b) Isometric view

(c) Longitudinal view

(d) Details of IRJ mesh

Figure 4.31 IRJ elastic zone meshing

Table 4.2 mesh of wheel/IRJ contact model

Part name		Number of elements	Number of nodes	Max size of elements in the refined zone
Wheel		56,606	65,865	2.5mm
IRJ	Beam part	46	48	230mm
	Railhead of solid part	56,625	63,080	0.5mm
	Rest of solid part	32,216	38,635	2.5mm

(a) Longitudinal view

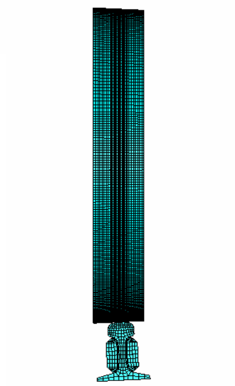

(b) End view

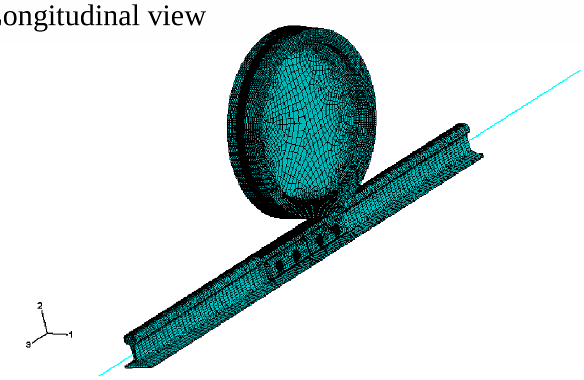

(c) Isometric view

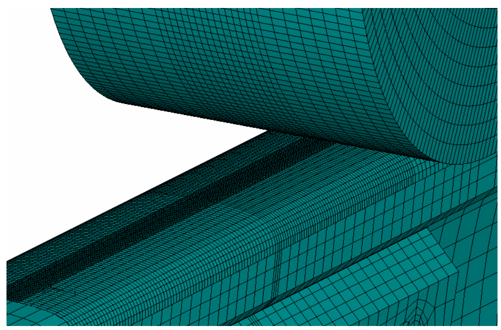

(d) Enlarged view for wheel/IRJ contact

Figure 4.32 Finite element meshing of the wheel-rail system

4.9. Summary

The FE modelling of wheel/rail contact impact in the vicinity of the end post has been introduced in this chapter. The 3D full scale wheel/rail contact model employs a two-step analysis strategy, from static to dynamic, to achieve a steady contact condition prior to impact analysis. To achieve a reasonable model size which is acceptable to the available computing facility, several model idealisation and simplification strategies are employed in following aspects:

- wheel profile and IRJ assembly
- material modelling
- boundary conditions

Some special attention is also paid to the following FE modelling strategies:

- loading strategy
- contact modelling strategy
- meshing strategy

With the employment of above strategies, the FE model is set up and the numerical example for wheel/rail contact impact at the IRJ is presented in next chapter.